



Response of dissolved organic matter optical properties to net inflow runoff in a large fluvial plain lake and the connecting channels

Yongqiang Zhou^{a,b,c}, Xiaolong Yao^{a,b}, Yunlin Zhang^{a,*}, Yibo Zhang^{a,b}, Kun Shi^a, Xiangming Tang^a, Boqiang Qin^a, David C. Podgorski^d, Justin D. Brookes^e, Erik Jeppesen^{c,f}

^a Taihu Laboratory for Lake Ecosystem Research, State Key Laboratory of Lake Science and Environment, Nanjing Institute of Geography and Limnology, Chinese Academy of Sciences, Nanjing 210008, China

^b University of Chinese Academy of Sciences, Beijing 100049, China

^c Sino-Danish Centre for Education and Research, Beijing 100190, China

^d Pontchartrain Institute for Environmental Sciences, Department of Chemistry, University of New Orleans, New Orleans, 70148, LA, USA

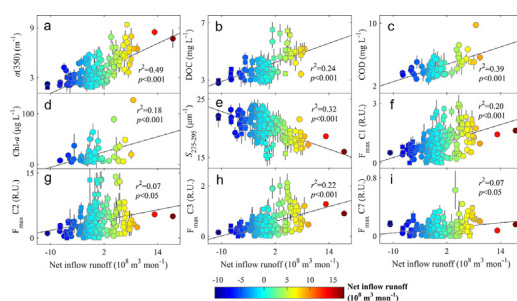
^e Water Research Centre, Environment Institute, School of Biological Science, University of Adelaide, 5005 Adelaide, Australia

^f Department of Bioscience and Arctic Research Centre, Aarhus University, Vejlsvøvej 25, DK-8600 Silkeborg, Denmark

HIGHLIGHTS

- Net water inflow varied greatly in different sub-watersheds of the Lake Taihu Basin.
- We found significant relationships between Q_{net} and CDOM optical properties.
- We found strong catchment and anthropogenic effects in various regions of Lake Taihu.
- Net water inflow controls the optical properties of CDOM molecules in Lake Taihu.

GRAPHICAL ABSTRACT



ARTICLE INFO

Article history:

Received 1 April 2018

Received in revised form 14 May 2018

Accepted 15 May 2018

Available online 26 May 2018

Editor: Kevin V. Thomas

Keywords:

Chromophoric dissolved organic matter (CDOM)

Parallel factor analysis (PARAFAC)

Fluvial plain lake

Net inflow runoff (Q_{net})

ABSTRACT

Fluvial plain lake watersheds are usually highly urbanized and have high concentrations of chromophoric dissolved organic matter (CDOM). CDOM derived from the connecting urban channels usually share strong terrestrial and anthropogenic signals and net inflow runoff (Q_{net}) to the lake serves as a proxy of residential household sewage input. We investigate how Q_{net} controls the optical characteristics of CDOM in fluvial plain Lake Taihu and the connecting channels. CDOM absorption coefficient $a(350)$, dissolved organic carbon (DOC), the fluorescence intensity (F_{max}) of seven PARAFAC components C1–C7, and $\delta^{15}N$ -TDN were higher in the northwestern relative to the other lake regions, and $a(250)/a(365)$, spectral slope $S_{275-295}$, and $\delta^{13}C$ -DOM relative low in the northwestern lake, all indicating strong terrestrial and anthropogenic effects. Conversely, the urban land cover (%Cities), gross domestic product (GDP), and population density were relatively low in the western sub-watersheds and high in the eastern sub-watersheds. This apparent paradox reflects variations in Q_{net} from different sub-watersheds. Thus, significant positive relationships were found between Q_{net} and $a(350)$, DOC, chemical oxygen demand (COD), chlorophyll-*a* (Chl-*a*), F_{max} of C1–C3 and C6–C7, and %C2–%C3 in the five hydraulic sub-watersheds. We revealed significant positive relationships between mean $a(350)$, DOC, COD, Chl-*a*, C1–C3 and C6, %C2–%C3, and the products of $Q_{net} \times \%Cities$, $Q_{net} \times GDP$, and $Q_{net} \times$ population density. We further found dominant contribution of lignin to the total number of assigned formulas for the samples

* Corresponding author at: Nanjing Institute of Geography and Limnology, Chinese Academy of Sciences, 73 East Beijing Road, Nanjing 210008, China.
E-mail address: ylzhang@niglas.ac.cn (Y. Zhang).

collected from the channels in the Huxi watershed and the central lake using high resolution mass spectroscopy. We conclude that Q_{net} is of key importance for the optical properties of CDOM molecules in the various regions of Lake Taihu and the connecting channels.

© 2018 Elsevier B.V. All rights reserved.

1. Introduction

Urbanization and industrialization usually take place in large fluvial plains and coastal lake watersheds, which support the livelihood of >75% of the human population worldwide (Paerl et al., 2013). An increase in the urban and agricultural land use results in increasing amounts of household sewage and agricultural humic-like substances that are discharged downstream (Williams et al., 2016; Williams et al., 2010). Fluvial plains are usually located at low altitude with elevations < 10 m, and lake watersheds drainage within these areas can be complex as the connecting river systems include natural rivers, semi-artificial-reformed rivers, man-made channels, and hundreds of floodgates. The resulting effect on the carbon loading of lakes can be complex and represents a challenge to unravel the sources of organic matter. Sewage derived from intensive residential areas in these ecosystems often contains high concentrations of dissolved organic matter (DOM).

Chromophoric DOM (CDOM) is the colored fraction of DOM that can strongly absorb light in the ultraviolet (UV) and blue regions. CDOM originates from terrestrial and anthropogenic organic matter, microbial degradation of aquatic organisms, and extracellular secretion released by algae, and consists of a complex mixture of organic molecules. Its translocation and transformation strongly impact the inland water carbon cycling and the outgassing of greenhouse gases (Davidson et al., 2018; Le et al., 2015; Stedmon and Markager, 2005a; Zhao et al., 2017). Numerous studies have elucidated how discharge impacts the dynamics of CDOM in streams, rivers, mountainous lakes, and estuaries (Guo et al., 2014; Huang et al., 2017; Li et al., 2016; Stedmon and Markager, 2005a; Yang et al., 2013; Zhao et al., 2016). In fluvial plain lake watersheds, however, the direction of flow in the lake and the connecting river networks are broadly similar to that of lagoons and can be reversed (backflow) under certain anthropogenic, climatic, and tidal conditions, and especially during cyclone events (Qin et al., 2007; Zhu et al., 2014). The hydraulic linkages between lakes and the connecting channels in fluvial plain lake watersheds are therefore much more complicated than mountainous lake ecosystems with fixed flow direction. However, there have been few attempts to characterize how net inflow runoff (Q_{net} , calculated as backflow runoff subtracting from inflow runoff) from connecting channels affects the variation in the optical properties of CDOM in fluvial plain lake ecosystems.

It is difficult to trace the concentration and compositional dynamics of CDOM due to the complex mix of CDOM molecules. UV-Vis spectral absorption and fluorescence measurements are important tools to evaluate the optical concentration and composition of CDOM molecules. CDOM fluorescent (FDOM) measurements of excitation (Ex) and emission (Em) matrices (EEMs) are easy to obtain and yield high optical resolution by enabling distinction of materials that absorb at the same wavelength but emit in different spectral regions (Murphy et al., 2008). Parallel factor analysis (PARAFAC) decomposes EEMs of complex mixture into distinct trilinear components and is useful in interpreting EEMs data arrays (Murphy et al., 2013; Stedmon and Bro, 2008). The stable isotopes $\delta^{13}\text{C}$ -DOM and $\delta^{15}\text{N}$ -TDN can be used to trace the sources of bulk DOM as, typically, $\delta^{13}\text{C}$ -DOM of terrestrial humic-rich DOM ranges between -29% and -26% , and is similar to that of terrestrial C3 plants with $\delta^{13}\text{C}$ -DOM ranges from -34% to -23% (Hood et al., 2009; Vizzini et al., 2005). In comparison, $\delta^{13}\text{C}$ -DOM of biological autochthonous DOM (microbial degradation of phytoplankton) typically ranges between -25% and -20% and is roughly similar to values for C4 plants (-23% to -7%) (Hood et al., 2009; Vizzini et al., 2005). $\delta^{15}\text{N}$ -TDN values were highest for riverine and anthropogenic input (Vizzini et al., 2005; Zhou et al., 2015b). Fourier transform ion cyclotron resonance mass spectrometry (FT-ICR MS) can be used to trace the

composition of DOM from the molecular level. FT-ICR MS enables the assignment of thousands of molecular formulas of DOM in various aquatic ecosystems (Kellerman et al., 2015; Spencer et al., 2014; Stubbins et al., 2010).

The Lake Taihu watershed is the most developed area in China with high population density, urbanization, and economic development (Qin et al., 2007). It covers 36,500 km², and the lake has an area of 2338.1 km² with a mean depth of 1.89 m. The lake bottom has a mean elevation of ~ 1.1 m above sea level and a total of 172 rivers or man-made channels are connected to the lake (Qin et al., 2007). The summed length of channels in the Lake Taihu watershed is 120,000 km, i.e. ~ 3.2 km km⁻² (Qin et al., 2007), and the water retention time of the lake is about 300 days (Tang et al., 2010). Water runoff usually drains from the west, passes through the lake and to the east, and finally empties into the East China Sea (Fig. 1). However, the water flow in the whole lake watershed can be reversed, i.e. backflow runoff; this is especially pronounced during the dry season (from late autumn to late spring) and occurs particularly in the eastern part of the lake watershed (Qin et al., 2007). Water flow directions of the channels connecting to Lake Taihu are largely controlled by tidal exchange, extreme events (typhoon passages), and anthropogenic disturbance (e.g. hundreds of floodgates), and are broadly similar to that of lagoon systems. Q_{net} draining to the lake from different hydraulic sub-watersheds can therefore be used to trace anthropogenic effluents from the corresponding sub-watersheds. High urban land cover (%Cities) in the Lake Taihu watershed result in a high nutrient and CDOM input, which boosts the outbreak of algal blooms, as well as the accumulation of high concentrations of autochthonous CDOM (Duan et al., 2014; Zhou et al., 2015a). High concentrations of CDOM can cause an unpleasant odor and taste of the water and produce undesirable disinfection byproducts during water treatment processes (Tomlinson et al., 2016). The lability of CDOM to degradation and mineralization is largely determined by its source and composition (Stedmon et al., 2007). Although there have been studies unraveling the spatial and temporal variations of CDOM optical properties in Lake Taihu (Yao et al., 2011; Zhang et al., 2011; Zhou et al., 2015b), how the Q_{net} from individual hydraulic sub-watersheds may influence the sources and optical properties of CDOM in the lake watersheds remains, however, largely unknown. It was found that the Q_{net} varied greatly between the individual hydraulic sub-watersheds of the Lake Taihu watershed (Qin et al., 2007).

In this study, we attempt to unravel how Q_{net} draining to the lake from individual hydraulic sub-watersheds may quantitatively control the optical properties of CDOM in the fluvial plain Lake Taihu watershed. A total of 2277 field samples (128 samples collected in 2011 were previously reported in reference Zhou et al. (2015b)) collected from the lake watershed from February 2008 to November 2016 and long-term data on the monthly (August 2009–December 2016) inflow and backflow runoff (net inflow, Q_{net}) in individual hydraulic sub-watersheds of the lake were used to elucidate how Q_{net} may influence the sources and optical properties of CDOM in the lake watersheds. We hypothesized that the Q_{net} from individual sub-watersheds controls the optical properties of CDOM and its variation in the lake and the connecting channels.

2. Materials and methods

2.1. Hydraulic sub-watersheds of Lake Taihu and hydrological and socio-economic data collection

The Lake Taihu watershed can be divided into seven individual hydraulic sub-watersheds according to the Taihu Basin hydrological

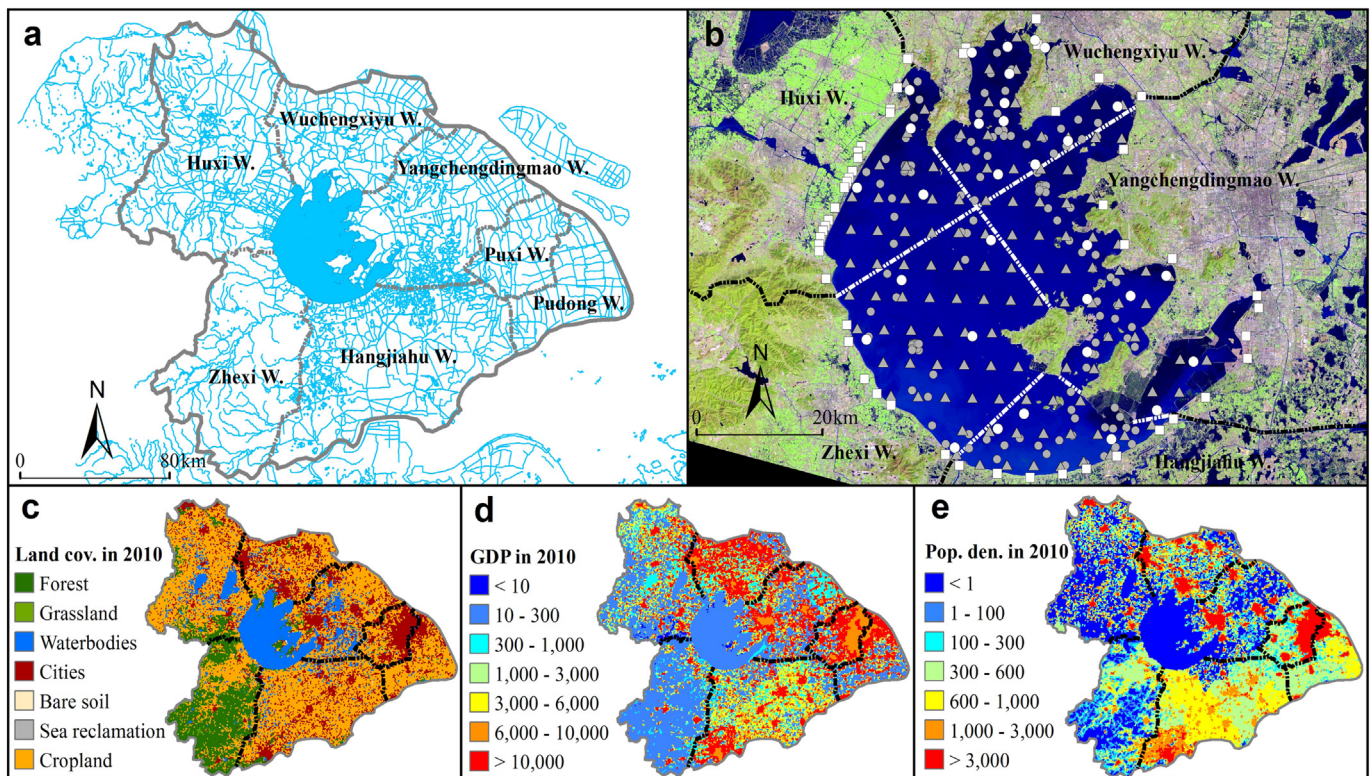


Fig. 1. Five sub-watersheds were delineated by gray dashed lines (a). Location of 32 seasonal sampling sites in Lake Taihu (white circles) from February 2008 to November 2016, 146 sites in October 2008 (gray circles), and 116 sites in January and June 2014, and June 2015 (gray triangles) (all sites were divided into five spatial subgroups delineated by white dashed lines following the boundaries of the five corresponding sub-watersheds), and location of 51 seasonal sampling sites on the connecting channels (white quadrates) from November 2013 to November 2016 (b). Land cover (c), gross domestic product (GDP, in 10^4 RMB yuan km^{-2} ; d), and population density (km^{-2} ; e) of the Lake Taihu Watershed in 2010.

information service system (<http://218.1.102.99:8100/indexWater.html>): Huxi, Wuchengxiyu, Zhexi, Hangjiahu, Yangchengdianmao, Pudong, and Puxi (Fig. 1). The hydraulic sub-watersheds were divided following the boundary where there is barely water exchange between neighboring sub-watersheds (<http://218.1.102.99:8100/indexWater.html>). The sub-watersheds Pudong and Puxi are not located in the catchment surrounding Lake Taihu (Fig. 1) and are therefore not further discussed. Five corresponding sub-regions surrounded by the five sub-watersheds in Lake Taihu were divided according to the boundary of the hydraulic sub-watersheds (Fig. 1).

In this study, inflow runoff is defined as inflow discharge from rivers or channels to Lake Taihu while backflow runoff is defined as backwaters discharged from the lake to the channels connecting to it. Q_{net} is calculated as inflow - backflow runoff and it is noted that $Q_{\text{net}} < 0$ denotes inflow runoff is less than the backflow runoff. Long-term data series on the monthly (August 2009–December 2016) inflow and backflow runoff from the five hydraulic sub-watersheds are available from the Taihu Basin hydrological information service system (<http://218.1.102.99:8100/indexWater.html>). Data on water flow direction in the lake itself are not available and not considered in this study.

Information on the land cover in 2005, 2010, and 2015 in the Lake Taihu watershed was extracted from 1 km resolution national land cover data for China identified through visual interpretation of Landsat TM images (available from <http://www.resdc.cn/>) with ArcGIS 10.2 software. The land cover classes were further categorized into seven groups: forest, grassland, waterbodies, cities, bare soil, sea reclamation, and cropland (Liu et al., 2005). Gross domestic product (GDP) and population density data in 2005 and 2010 with a spatial resolution of 1 km (available from <http://www.resdc.cn/>) for the Lake Taihu watershed were extracted using ArcGIS 10.2 software. Because of limited temporal resolution, land cover, GDP, and population density in 2005 were used to represent 2008–2009, and 2010 to represent 2010–2014, and 2015 to represent 2015–2016 and correlated with CDOM-related indices. It

is noted that GDP and population density data in 2015 is not available and we used the data in 2010 to represent.

2.2. Field sampling collection

A total of 2277 field samples were collected from the Lake Taihu watershed - 663 from 51 major channels connecting to the lake (0.2–5 km upstream of the river mouths) and the remaining 1614 from the lake. The 663 river samples were collected seasonally (February, May, August, and November every year) from November 2013 to November 2016 and among the remaining 1614 lake samples, 1120 were collected seasonally (February, May, August, and November every year) from February 2008 to November 2016 (data are unavailable in February 2010), 146 in October 2008, and 348 (116×3) in January and June 2014 (Fig. 1). Surface (0–0.5 m) water samples were taken with 5 L acid-cleaned Niskin bottles and stored on ice while in the field. The samples were filtered in the laboratory no later than 2 h after sampling and stored in the dark at 4 °C. CDOM absorption and fluorescence measurements were usually completed within three days and all laboratory measurements were finished within five days.

2.3. CDOM absorption and fluorescence measurements

The water samples were first filtered through pre-combusted (450 °C for 4 h) Whatman GF/F filters (0.7 μm porosity) and then through pre-rinsed Millipore membrane cellulose filters (0.22 μm) under low pressure into acid-cleaned and pre-combusted (550 °C for 6 h) glass bottles. CDOM absorbance spectra were obtained between 200 and 800 nm at 1 nm intervals on a Shimadzu UV-2550PC UV-Vis spectrophotometer with matching 5 cm quartz cells. Measurements were performed at room temperature (20 ± 2 °C) and Milli-Q water was used in the reference cell. Absorbance spectra were baseline corrected by subtracting the absorbance at 700 nm. CDOM absorption was calculated

by multiplying absorbance by $2.303/r$, where r is the cuvette length (in m). The absorption coefficient at 350 nm, $a(350)$, is widely used in various ecosystems as an indicator of relative CDOM concentration (Stedmon et al., 2007; Yamashita et al., 2010) and was used in this study as a surrogate for CDOM concentration. We used the ratio $a(250)/a(365)$ to estimate the relative molecular size of CDOM (Helms et al., 2008) as previous studies have proved that this increases with decreasing $a(250)/a(365)$ (Helms et al., 2008). CDOM spectral slope ($S_{275-295}$) was calculated from the absorption spectra by nonlinear fitting (Helms et al., 2008). Similar to $a(250)/a(365)$, $S_{275-295}$ increased with decreasing molecular size of CDOM molecules, and an enhanced microbial reworking or photobleaching of CDOM molecules will result in increased $S_{275-295}$ (Fichot and Benner, 2012; Helms et al., 2008).

FDOM EEMs measurements were conducted on a F-7000 fluorescence spectrometer (Hitachi High Technologies, Tokyo, Japan) equipped with a xenon lamp (700 V) at room temperature. The Ex and Em scanning ranges were set to 200–450 nm (5 nm intervals) and 250–600 nm (1 nm intervals), respectively. The EEMs scanning speed was set to 2400 nm min⁻¹. Daily measurements of Milli-Q water were used as references. The EEM spectra measurements were corrected for instrumental biases according to the procedure recommended by Hitachi. Water Raman scatter peaks were eliminated by subtracting the EEMs of Milli-Q water blanks. Inner-filter effects on EEM measurements were removed by adjusting for CDOM absorbance at the corresponding wavelengths (Kothawala et al., 2013; Mcknight et al., 2001):

$$F_{\text{cor}} = F_{\text{obs}} \times 10^{(A_{\text{Ex}} + A_{\text{Em}})/2} \quad (1)$$

where F_{cor} and F_{obs} are the fluorescence intensity of EEMs pre- and post-calibration, respectively; and A_{Ex} and A_{Em} are the corrected absorbance at the corresponding Ex and Em wavelengths, respectively. Rayleigh scatter peaks were removed by interpolation using the drEEM toolbox (Murphy et al., 2013). Daily lamp variations were normalized to the integral of the Raman signal (Ex wavelength at 350 nm) of corresponding daily Milli-Q water samples to produce intensities of Raman units (R.U.) (Lawaetz and Stedmon, 2009). Data collected at Ex wavelengths below 230 nm and at Em wavelengths below 300 nm and above 550 nm were removed before further processing due to deteriorating signal-to-noise ratios.

2.4. PARAFAC modeling

PARAFAC is the method of choice for analysis of three-way data. In this case the EEM data consists of measurements for fluorescence at 251 excitation wavelengths, 45 emission wavelengths and 2227 samples. PARAFAC modeling was performed with the drEEM toolbox (ver. 0.2.0) in MATLAB R2015b (Murphy et al., 2013), which employs the

N-way toolbox as the engine of the PARAFAC algorithm (Andersson and Bro, 2000). The data array was split into six random dataset “halves” (three for calibration and three for validation) and four- to eight-component models were developed for each, yielding three “S₄C₆T₃” validation tests (Murphy et al., 2013). A seven-component model was well validated by split-half analysis, random initialization analysis, and analysis of residuals (Murphy et al., 2013; Stedmon and Bro, 2008), and it was found to adequately describe the whole EEMs data array (Fig. 2; Fig. S1; Fig. S2).

2.5. Fourier transform ion cyclotron resonance mass spectrometry (FT-ICR MS) measurements and data processing

A large fraction of DOM does not fluoresce after being excited with UV light and FT-ICR MS can be a promising tool to trace the molecular composition of DOM molecules across ecosystems (Kellerman et al., 2015; Spencer et al., 2014; Stubbins et al., 2010). In this study, a head-water sample, a river water sample in the Huxi watershed, and a water sample collected from Lake Taihu center were solid phase extracted using PPL Bond Elut (Agilent) resins following the methods detailed in Spencer et al. (2014). Briefly, ~50 mL water samples through Millipore membrane cellulose filters were acidified to pH = 2 using reagent grade HCl. The PPL columns were pre-cleaned by passing 3 mL methanol (ULC-MS grade), 6 mL Milli-Q water, and then again 3 mL methanol and sealed and soaked overnight with ~1.5 mL methanol in the columns, and thereafter rinsed with 3 mL 0.01 M HCl, 3 mL methanol, and 3 mL 0.01 M HCl in sequence. Calculated volumes of acidified water sample (approximately 60 µg C) were passed through each column at a flow rate of ~0.5 mL min⁻¹. Two columns of 0.01 M HCl were used to rinse the columns again to wash away any inorganic matter before the PPL columns were finally dried under high purity N₂ gas. DOM was eluted from the columns using 1 mL of methanol. The methanol extracts were diluted 1:1 with Milli-Q water and analyzed in negative mode electrospray ionization using a 21 Tesla FT-ICR MS. Molecular formulas were assigned to signals > 6σ RMS baseline noise using EnviroOrg ©,™ (Corilo, 2015) and the mass precision of the assigned formulas < 0.3 ppm after the instrument internal calibration.

The assigned formulas were categorized following the methods detailed in Ohno et al. (2014). The chemical compound categorized using the van Krevelen diagrams usually include: (a) lipids (O/C = 0–0.3, H/C = 1.5–2.0), (b) proteins and amino sugars (O/C = 0.3–0.67, H/C = 1.5–2.2), (c) lignins (O/C = 0.1–0.67, H/C = 0.7–1.5), (d) carbohydrates (O/C = 0.67–1.2, H/C = 1.5–2.2), (e) unsaturated hydrocarbons (O/C = 0–0.1, H/C = 0.7–1.5), (f) condensed aromatics (O/C = 0–0.67, H/C = 0.2–0.7), and (g) tannins (O/C = 0.67–1.2, H/C = 0.5–1.5) (Ohno et al., 2014).

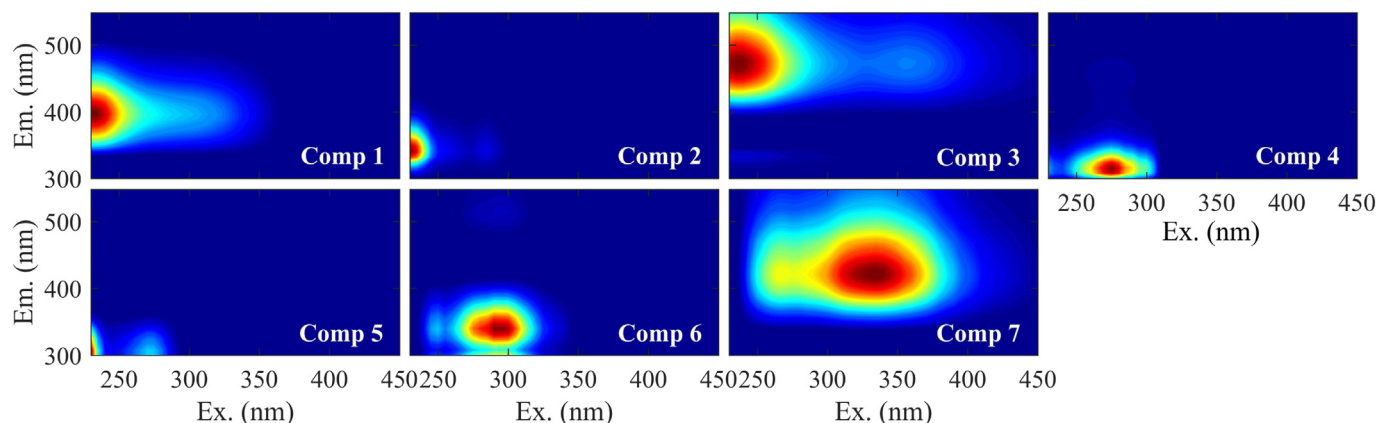


Fig. 2. Spectral characteristics of the seven PARAFAC components; the model was well validated using the split-half validation procedure (see Fig. S1).

2.6. Dissolved organic carbon (DOC), chemical oxygen demand (COD), chlorophyll-*a* (Chl-*a*) and stable isotopic measurements

Water samples filtered through Whatman GF/F filters were first acidified with 10 μL of 85% H_3PO_4 before DOC concentrations were determined by high temperature (680 $^\circ\text{C}$) combustion on a TOC-V CPN (Shimadzu, Tokyo, Japan) analyzer. DOC concentrations were not available for the samples collected before February 2013 except for the campaign in October 2008 (146 sites).

Water samples through GF/F filters were further measured for chemical oxygen demand (COD) by a colorimetric method using potassium dichromate sulfuric acid as reagent following the method detailed in Yao et al. (2011). COD concentrations were available for the samples collected from Lake Taihu seasonally from February 2011 to November 2014. Chlorophyll-*a* (Chl-*a*) concentration was determined spectrophotometrically at 665 and 750 nm by extraction using hot ethanol (90% at 80 $^\circ\text{C}$), and Chl-*a* was used in this study as a surrogate of algal biomass. Chl-*a* was available for the samples collected from the lake seasonally from February 2012 to November 2014.

Bulk $\delta^{13}\text{C}$ -DOM was determined for the samples collected from three sites (riverine, river mouth, and open water) from three major inflowing rivers: Changdou, Dapu, and Yincun in May 2010, February and August 2011, February, May, and August 2012 (see reference (Zhou et al., 2015b) for location details), and from the lake in November 2016. $\delta^{15}\text{N}$ -TDN was determined for the sample collected from the lake in November 2016. Water samples for $\delta^{13}\text{C}$ -DOM and $\delta^{15}\text{N}$ -TDN measurements were first poured through Whatman GF/F filters and then dried at low temperature (55 ± 5 $^\circ\text{C}$, generally within three days) in acid-cleaned beakers until constant weight. We used 12 M HCl (grade quality) to steam acidify the solid residue, i.e. DOM, for 72 h to remove dissolved inorganic matter. The solid residue was dried at low temperature again for 24 h and then stored in a desiccator and combusted on a Flash EA1112 analyzer. CO_2 and N_2 gases were measured with a Thermo Finnigan MAT Delta^{plus} dual-inlet continuous flow isotope ratio mass spectrometer with $<0.1\%$ precision for both $\delta^{13}\text{C}$ -DOM and $\delta^{15}\text{N}$ -TDN. $\delta^{13}\text{C}$ -DOM and $\delta^{15}\text{N}$ -TDN were calibrated against the Vienna Pee Dee Belemnite (VPDB) standard and high-purity N_2 gas, respectively (Hood et al., 2009; Zhou et al., 2015b).

2.7. Statistical analyses

Spatial variability of sampling sites and CDOM-related indices were mapped with ArcGIS 10.2 software. Linear fittings was performed with MATLAB R2015b. Mean, standard deviation, *t*-test, and the significance level of linear regressions were conducted using R i386 2.15.2. Results with linear fittings and *t*-test results with $p < 0.05$ were reported as significant.

3. Results

3.1. PARAFAC results

The seven-component model explained $>99.9\%$ of the total variability of the EEMs data array and was well validated using the split-half validation procedure (Fig. 2; Fig. S1; Fig. S2). The spectral shapes of the seven PARAFAC components (C1–C7) were compared with published models of other ecosystems using an online spectral library called Openfluor (Murphy et al., 2014). C1 (Ex/Em = $\leq 230/396$) was similar to microbial humic-like substances (Kothawala et al., 2014; Murphy et al., 2011; Shutova et al., 2014). C2 (Ex/Em = $\leq 230 (285)/340$) and C6 (Ex/Em = $250 (290)/340$) both displayed spectral shapes congruent with amino-acid-associated tryptophan-like components (Murphy et al., 2011; Shutova et al., 2014). C3 (Ex/Em = $235 (355)/476$) was characterized as representing typical terrestrial humic-like fluorophores (Shutova et al., 2014; Stedmon and Markager, 2005b; Williams et al., 2010). C4 (Ex/Em = $275/316$) and C5 (Ex/Em = $\leq 230 (270)/300$)

were both categorized as tyrosine-like components (Graeber et al., 2012; Kowalczyk et al., 2013; Yamashita et al., 2013), C4 being somewhat red shifted. C7 (Ex/Em = $265 (335)/420$) was similar to agricultural humic-like substances or red-shifted microbial humic-like material (Osburn et al., 2016; Stedmon and Markager, 2005a).

3.2. Hydrological conditions

Inflow and backflow runoff varied greatly among sub-watersheds (Fig. 3). Long-term (August 2009–December 2016) mean monthly inflow runoff to Lake Taihu from the five sub-watersheds ranged from $0.3 \pm 0.3 \times 10^8 \text{ m}^3 \text{ month}^{-1}$ (Yangchengdingmao) to $6.2 \pm 3.1 \times 10^8 \text{ m}^3 \text{ month}^{-1}$ (Huxi), and monthly backflow runoff ranged from $0.2 \pm 0.4 \times 10^8 \text{ m}^3 \text{ month}^{-1}$ (Huxi) to $4.6 \pm 3.0 \times 10^8 \text{ m}^3 \text{ month}^{-1}$ (Yangchengdingmao) (Table S1). Correspondingly, monthly mean Q_{net} of the aforementioned five sub-watersheds ranged from $-4.3 \pm 3.0 \times 10^8 \text{ m}^3 \text{ month}^{-1}$ (Yangchengdingmao) to $6.0 \pm 3.2 \times 10^8 \text{ m}^3 \text{ month}^{-1}$ (Huxi) (a negative Q_{net} “-” denotes backflow runoff $>$ inflow runoff; Fig. 3; Table S1).

3.3. Land cover, GDP, and population density results

To a certain extent, %Cities can be used as a proxy for discharge of household sewage from the residential areas of the individual sub-watersheds. In 2005, %Cities in the five sub-watersheds surrounding Lake Taihu ranged from 3.2% (Zhexi) to 27.2% (Wuchengxiyu); in 2010, %Cities in the five sub-watersheds ranged from 3.7% (Zhexi) to 32.8% (Wuchengxiyu); and in 2015, %Cities ranged from 5.0% (Zhexi) to 34.6% (Wuchengxiyu) (Fig. S3; Table S2).

In 2005, the mean GDP of the five sub-watersheds ranged from $728 \times 10^4 \text{ RMB yuan km}^{-2}$ (US\$: $115 \times 10^4 \text{ km}^{-2}$, Zhexi; the exchange rate on 27 April 2018 when 1 US\$ = ~ 6.33 RMB yuan) to $8375 \times 10^4 \text{ RMB yuan km}^{-2}$ (US\$: $1323 \times 10^4 \text{ km}^{-2}$, Wuchengxiyu), and in 2010, the mean GDP of the five sub-watersheds ranged from $1466 \times 10^4 \text{ RMB yuan km}^{-2}$ (US\$: $232 \times 10^4 \text{ km}^{-2}$, Zhexi) to $11,708 \times 10^4 \text{ RMB yuan km}^{-2}$ (US\$: $1850 \times 10^4 \text{ km}^{-2}$, Wuchengxiyu) (Fig. S3; Table S2).

The mean population density of the five sub-watersheds ranged from 325 km^{-2} (Zhexi) to 1770 km^{-2} (Wuchengxiyu) in 2005, and in 2010, the mean population density ranged from 344 km^{-2} (Zhexi) to 1427 km^{-2} (Wuchengxiyu) (Fig. S3; Table S2).

3.4. Spatial variability of CDOM quantity and quality, COD, Chl-*a*, and stable isotopic signatures

There were notable differences among the CDOM optical properties for the samples collected from the channels in different sub-watersheds despite all samples share strong anthropogenic EEMs signals (Fig. S4; Table S3). In this study, $a(350)$ serves as a surrogate to trace the relative concentrations of CDOM as data on DOC concentrations were unavailable before February 2013, except for the campaign in October 2008. $a(350)$ decreased notably from the northwestern bays to the southeastern bays (Fig. S5), and high levels of $a(350)$ were found in the northwestern bay in all seasons (Fig. S5). $S_{275-295}$ can be used to trace the relative molecular size of CDOM molecules (Fichot and Benner, 2012; Helms et al., 2008), and it increased notably from the northwestern bays to the southeastern bays in all seasons (Fig. S5).

Multi-year (February 2008 to November 2016) mean contribution percentages of the seven PARAFAC components (%C1–%C7) were 12.4%, 38.7%, 6.0%, 24.0%, 11.1%, 6.5%, and 1.4%, respectively. For all sampling campaigns, the F_{max} of all the seven components, except for the two tyrosine-like C4 and C5, decreased notably from the northwestern bays to the southeastern bays (Fig. S6). High values of C4 and C5 were found in the northern half of the lake and western coastal lines, respectively (Fig. S6). PARAFAC-derived C3 is an exclusive terrestrial humic-like fluorophore (Fig. 2) and can be used to trace terrestrial organic

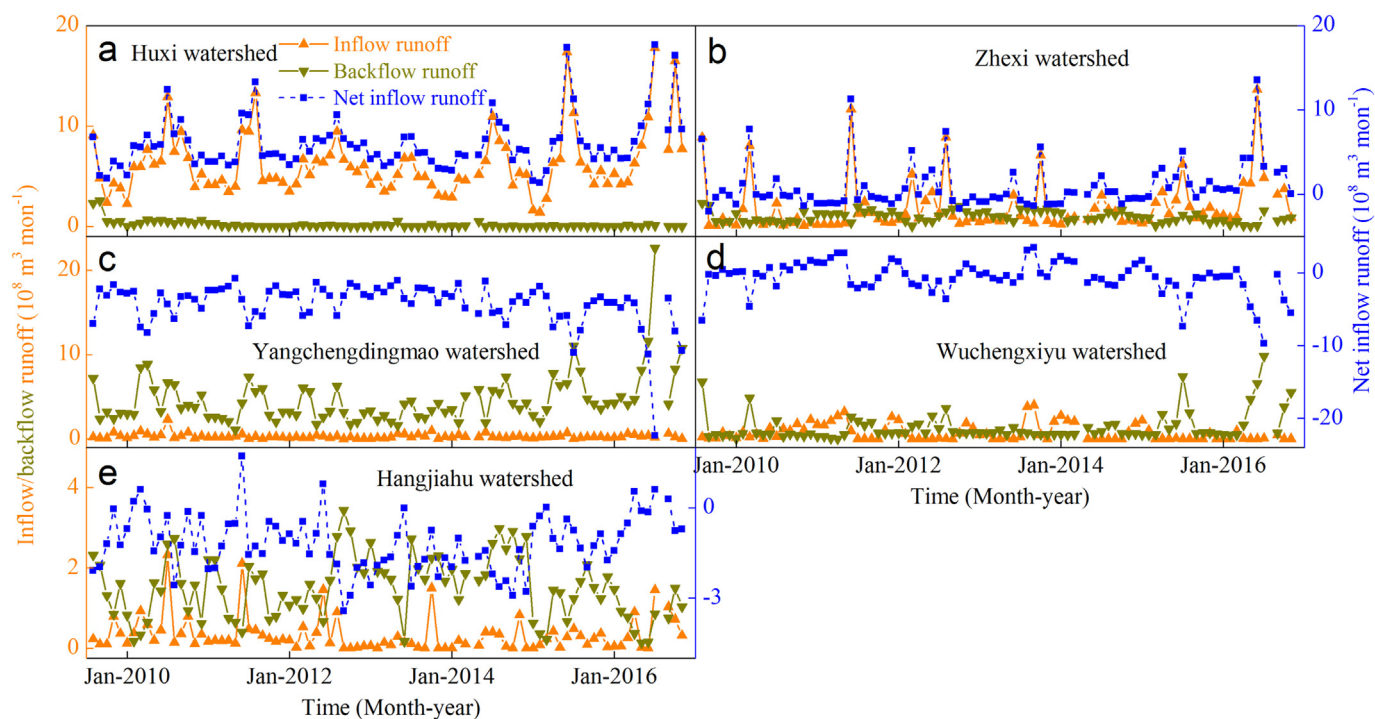


Fig. 3. Long-term monthly (August 2009–November 2016) inflow and backflow runoff and the corresponding monthly net inflow runoff (Q_{net}) for the Huxi (a), Zhexi (b), Yangchengdingmao (c), Wuchengxiyu (d), and Hangjiahu (e) watersheds.

matter input. $a(350)$ ($r^2 = 0.23$), DOC ($r^2 = 0.56$), C1 ($r^2 = 0.75$), C2 ($r^2 = 0.48$), C4 ($r^2 = 0.13$), C5 ($r^2 = 0.20$), and C6 ($r^2 = 0.12$) are all significantly and positively correlated to C3. High levels of F_{max} of C3 were found in the northwestern bay in all seasons (Fig. 4). The contribution percentage of humic-like components (C1, C3, and C7) to the summed F_{max} of the seven PARAFAC components (C_{humics}) can be used to trace the transition between waters dominated by humic-rich sources vs internal biological production. C_{humics} decreased notably from the northwestern bays to the southeastern lake regions in all seasons (Fig. 4).

Apart from C3, DOC were significantly and positively correlated to $a(350)$ ($r^2 = 0.55$; Fig. S7; Fig. S8), microbial humic-like C1 ($r^2 = 0.50$; Fig. S7; Fig. S8), tryptophan-like C2 ($r^2 = 0.23$; Fig. S7; Fig. S8) and C6 ($r^2 = 0.08$; Fig. S7; Fig. S8), and agricultural or red-shifted microbial humic-like C7 ($r^2 = 0.10$; Fig. S7; Fig. S8). No significant relationship was found between DOC and tyrosine-like C4 and C5 (Fig. S7; Fig. S8). Similar with $a(350)$ and terrestrial humic-like C3, DOC decreased notably from the northwestern bays to the southeastern bays in all seasons.

COD for the samples collected from Lake Taihu ranged from 2.43 to 15.56 $mg\ L^{-1}$ with a mean of $4.35 \pm 1.43\ mg\ L^{-1}$ (Fig. 4). In comparison, Chl-*a* concentrations in the lake ranged from 1.2 to 270.6 $\mu g\ L^{-1}$ with a mean of $20.2 \pm 28.6\ \mu g\ L^{-1}$ (Fig. 4). Both COD and Chl-*a* decreased notably from northwestern bay to southeastern bays with high values recorded in the northwestern half of the lake, especially in the northwestern inflowing river mouths in all seasons (Fig. 4). COD were significantly and positively correlated to DOC ($r^2 = 0.37$; Fig. S9), $a(350)$ ($r^2 = 0.37$; Fig. S9), microbial humic-like C1 ($r^2 = 0.12$; Fig. S9), terrestrial humic-like C3 ($r^2 = 0.18$; Fig. S9), and negatively correlated to $a(250)/a(365)$ ($r^2 = 0.23$; Fig. S9), and $S_{275-295}$ ($r^2 = 0.37$; Fig. S9).

Multi-year mean (May 2010 to August 2012) bulk $\delta^{13}C$ -DOM for the samples collected from the three river profiles ranged from -27.1% to -25.1% with a mean of $-26.3 \pm 0.4\%$ (Fig. 5). Paired *t*-test results indicated that there was no significant difference between the mean $\delta^{13}C$ -DOM of riverine sample and open water sample in any one of the three river profiles (Fig. 5). No significant seasonal variation was found in the mean $\delta^{13}C$ -DOM of any one of the three river profiles (Fig. 5). In November 2016, bulk $\delta^{13}C$ -DOM of all field sampling sites ranged from -27.5% to -25.2% , with a mean of $-26.2 \pm 0.4\%$ (Fig. 5). $\delta^{13}C$ -

DOM values increased gradually from the northwestern bays to the southeastern bays (Fig. 5). In comparison, in November 2016, bulk $\delta^{15}N$ -TDN ranged from -0.8% to 13.8% , with a mean of $6.6 \pm 3.2\%$ (Fig. 5). Bulk $\delta^{15}N$ -TDN decreased notably from the northwestern bays to the southeastern bays (Fig. 5).

3.5. Relationships between Q_{net} and CDOM-related indices

Significant positive relationships were observed between monthly Q_{net} in the five sub-watersheds of the lake and monthly mean $a(350)$, DOC, COD, Chl-*a*, and F_{max} of C1–C3 and C7 ($r^2 = 0.07$, $p < 0.05$) at the five corresponding lake and river sites (Fig. 6; Table 1). Significant negative relationships were recorded between monthly Q_{net} in the five sub-watersheds of the Lake Taihu watershed and monthly mean $a(250)/a(365)$ and $S_{275-295}$ at the five corresponding lake and river sites (Fig. 6; Fig. S10). No significant relationships were, however, traced between monthly mean Q_{net} in the five sub-watersheds and monthly mean F_{max} of tyrosine-like C4 and C5, and tryptophan-like C6 at the five corresponding lake and river sites (Fig. S10). It is noted that there is no significant relationship between Chl-*a* and F_{max} of the seven components except for C7 ($r^2 = 0.24$, $p < 0.001$; Fig. S11).

Significant positive relationships were also observed between the products of monthly $Q_{net} \times \%Cities$ and mean $a(350)$, DOC, COD, Chl-*a*, C1–C3, and C7 in the five sub-watersheds (Fig. 7; Table 1). Similarly, significant positive relationships were found between the products of monthly $Q_{net} \times GDP$, and $Q_{net} \times population\ density$ and $a(350)$, DOC, Chl-*a*, and C1–C3 (Fig. 7; Table 1). In comparison, significant negative relationships were observed between the products of monthly $Q_{net} \times \%Cities$, $Q_{net} \times GDP$, and $Q_{net} \times population\ density$ and mean $a(250)/a(365)$, $S_{275-295}$ in the associated catchment (Fig. 7; Table 1). No significant relationship was recorded between the products of monthly $Q_{net} \times \%Cities$, $Q_{net} \times GDP$, and $Q_{net} \times population\ density$ and the two tyrosine-like C4 and C5 (Table 1).

Significant positive relationships were found between monthly Q_{net} , the products of monthly $Q_{net} \times GDP$, and $Q_{net} \times population\ density$ and $\%C2$ and $\%C3$ (Fig. 8; Table S4). In comparison, significant negative relationships were observed between monthly Q_{net} , the products of

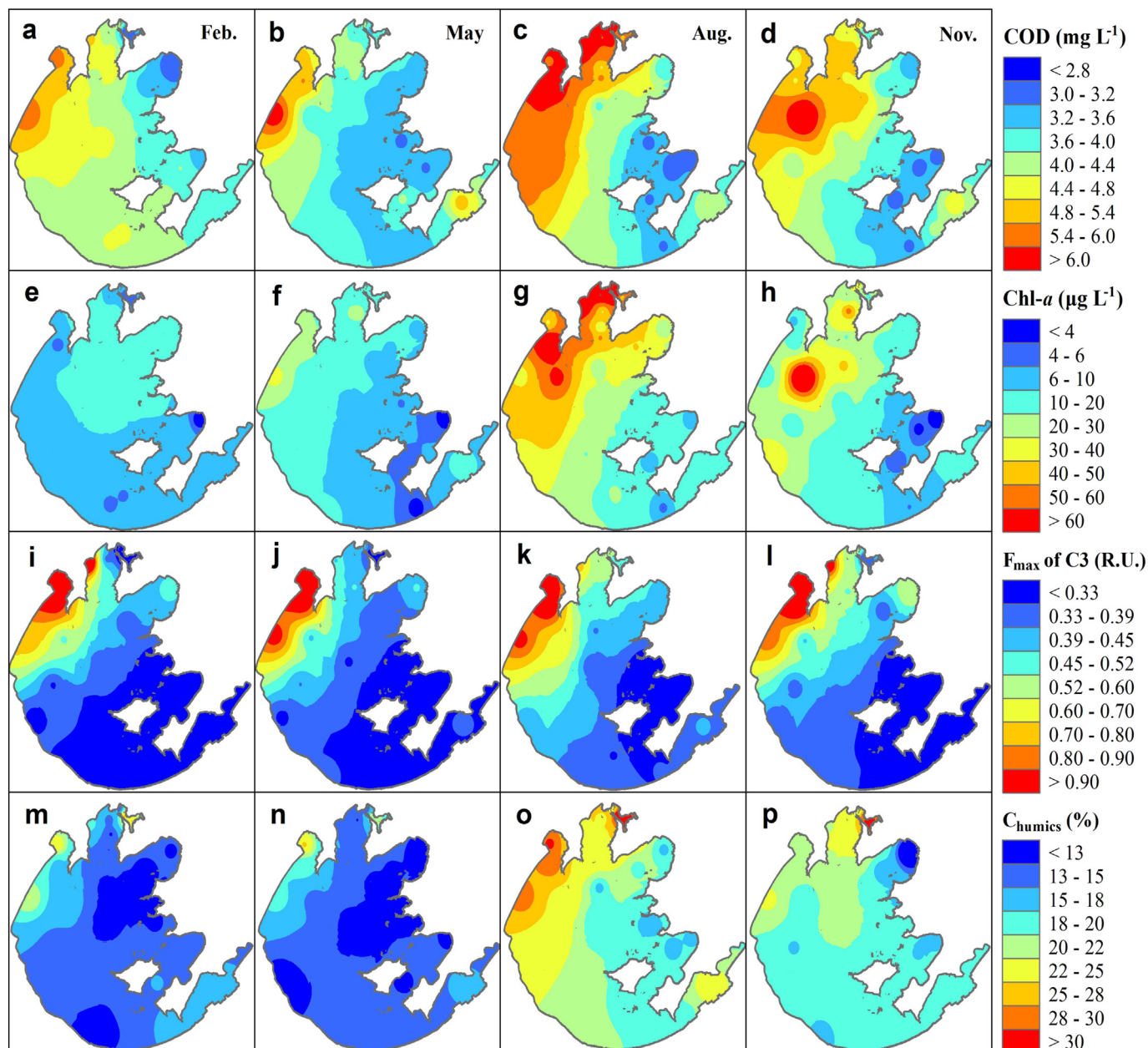


Fig. 4. Spatial distribution of multi-year mean chemical oxygen demand (COD, from February 2011 to November 2014, a–d), chlorophyll-*a* (Chl-*a*, from February 2012 to November 2014, e–h), F_{\max} of terrestrial humic-like C3 (February 2008–November 2016, i–l), and the contribution percentage of humic-like components (February 2008–November 2016, m–p).

monthly $Q_{\text{net}} \times \text{GDP}$, and $Q_{\text{net}} \times \text{population density}$ and $a(250)/a(365)$, $S_{275-295}$, %C4 (Fig. 8; Fig. S12; Table 1; Table S4). No significant relationship was recorded between monthly Q_{net} , the products of monthly $Q_{\text{net}} \times \text{GDP}$, and $Q_{\text{net}} \times \text{population density}$ and %C1, %C5, %C6, and %C7 (Fig. S12; Table S4).

3.6. FT-ICR MS results

Solid-phase extracted samples for the headwater sample in the Lake Taihu watershed, river sample in the Huxi watershed, and the lake center sample contained between 4315 and 9867 peaks with molecular formulas were assigned (Fig. 9; Table S5). In total, lignin displayed 3331, 6936, and 3245 assigned formula peaks, corresponding to 77%, 70%, and 68% for the headwater sample, the inflowing river sample in the Huxi watershed, and the central lake sample (Fig. 9; Table S5). In comparison, protein displayed 214, 1376, and 961 assigned formula peaks,

corresponding to 5%, 14%, and 16% for the headwater, the inflowing river and lake DOM samples in the Huxi watershed, and the central lake sample (Fig. 9; Table S5). All samples contained high proportions of carbohydrates (CHO) (46%–49%) and nitrogen-containing compounds (CHON) formulas (47%–50%; Fig. 9). The proportions of sulphur-containing compounds (CHOS) formulas for the three different sources of DOM samples ranged from 2% to 5% (Fig. 9).

4. Discussion

The optical characteristics of CDOM in various regions of Lake Taihu and the connecting channels are strongly influenced by Q_{net} from the corresponding sub-watersheds. We found that $a(350)$, DOC, COD, Chl-*a*, and F_{\max} of C1–C3 and C6–C7 was particularly high in the north and north-western regions. Moreover, $a(250)/a(365)$ and $S_{275-295}$ (decreases with increasing aromaticity of CDOM molecules (Fichot and

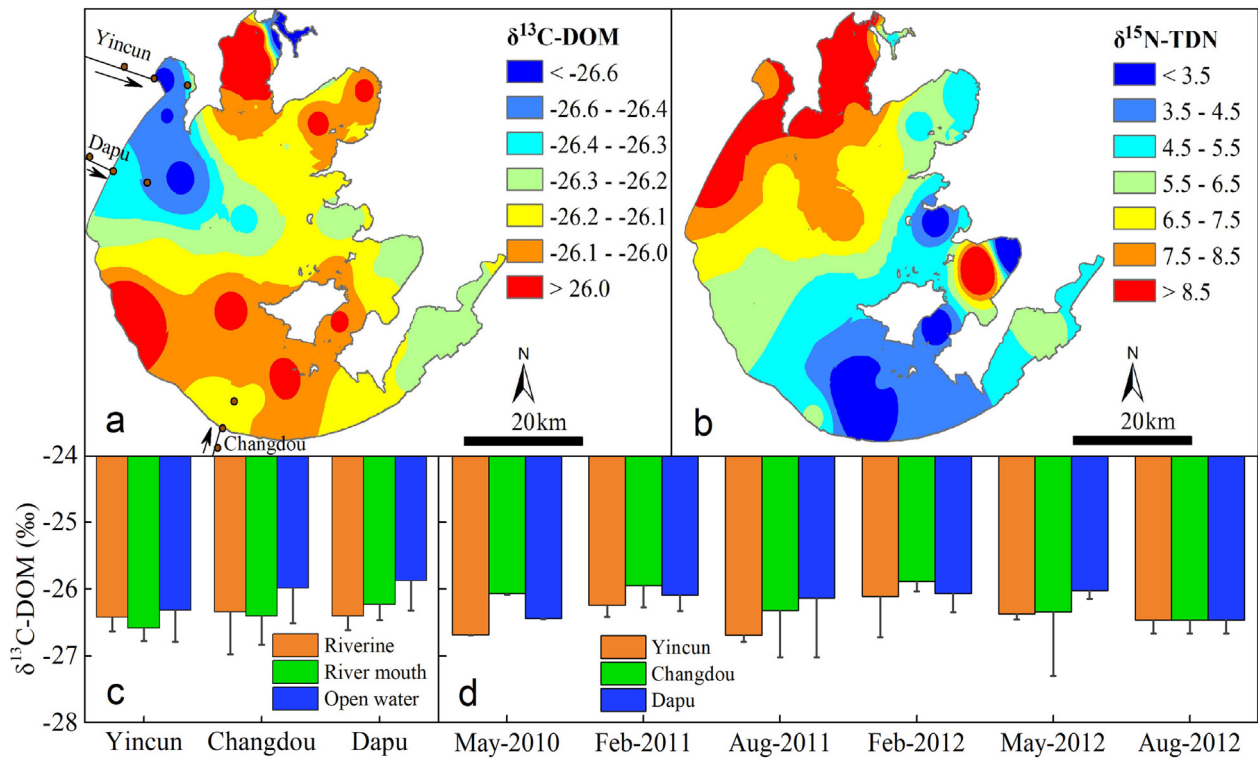


Fig. 5. Spatial distribution of stable isotopes $\delta^{13}\text{C}$ -DOC and $\delta^{15}\text{N}$ -TDN in the samples collected from Lake Taihu in November 2016 (a-b). Multi-year (May 2010 – August 2012) mean $\delta^{13}\text{C}$ -DOC collected from the three river profiles (Yincun, Dapu, and Changdou, c) and the corresponding long-term variations (d).

Benner, 2012; Helms et al., 2008)) were low and $\delta^{13}\text{C}$ -DOM was depleted in these regions. This suggests high input from the terrestrial environment, despite a relatively low urban land cover, GDP, and

population density in the North and Western sub-watersheds (Fig. 1; Fig. S3), but coinciding well with high Q_{net} in these regions. Enriched $\delta^{15}\text{N}$ -TDN and high COD (Fig. 5) further indicate major anthropogenic

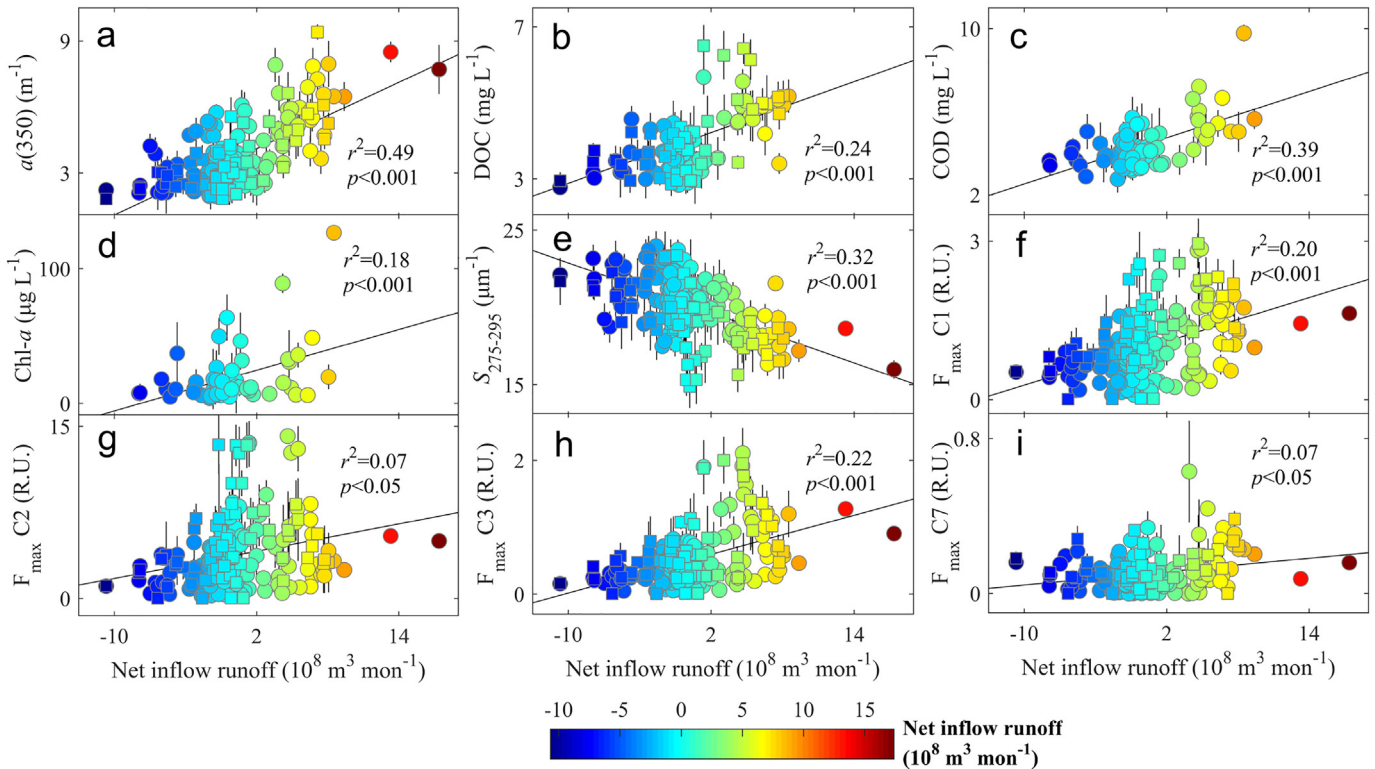


Fig. 6. Relationships between monthly net inflow runoff (Q_{net}) and CDOM absorption coefficient $a(350)$ (a), DOC (b), chemical oxygen demand (COD, c), chlorophyll- a (Chl- a , d), CDOM absorption spectral slope $S_{275-295}$ (e), and F_{max} of PARAFAC-derived C1–C3, and C7 (f–i) collected from five lake regions and the connecting channels delineated by dashed lines as shown in Fig. 1. Circles represent the samples collected from the lake and quadrates stand for the samples collected from the connecting channels. Error bars in all panels represent ± 1 S.D. of samples collected from the five lake regions.

Table 1

Determination coefficients and significance levels of linear relationships between CDOM-related indices and net inflow discharge (Q_{net}), and the products of $Q_{\text{net}} \times$ urban land cover (%Cities), the products of monthly $Q_{\text{net}} \times$ gross domestic products (GDP), and the products of $Q_{\text{net}} \times$ population density for the samples collected from the five lake regions and connecting channels shown in Fig. 1 from February 2008 to November 2016. *: $p < 0.05$.

CDOM indices	$a(350)$	DOC	COD	Chl- a	$a(250)/a(365)$	$S_{275-295}$	C1
Q_{net}	0.49*	0.38*	0.39*	0.18*	0.26*	0.32*	0.20*
$Q_{\text{net}} \times$ %Cities	0.38*	0.19*	0.30*	0.12*	0.19*	0.25*	0.18*
$Q_{\text{net}} \times$ GDP	0.32*	0.16*	0.24*	0.09*	0.16*	0.23*	0.16*
$Q_{\text{net}} \times$ Pop. den.	0.39*	0.19*	0.29*	0.12*	0.19*	0.24*	0.18*
CDOM indices	C2	C3	C4	C5	C6	C7	
Q_{net}	0.07*	0.22*	0.00	0.00	0.06	0.07*	
$Q_{\text{net}} \times$ %Cities	0.08*	0.20*	0.01	0.00	0.06	0.03	
$Q_{\text{net}} \times$ GDP	0.08*	0.18*	0.01	0.00	0.06	0.02	
$Q_{\text{net}} \times$ Pop. den.	0.08*	0.21*	0.01	0.00	0.06	0.03	

$a(350)$: CDOM absorption at 350 nm; DOC: dissolved organic carbon; COD: chemical oxygen demand; Chl- a : chlorophyll- a ; $S_{275-295}$: CDOM absorption spectral slope; $I_C:I_T$: fluorescence peak integration ratio; C1-C7: the seven PARAFAC components.

input from household sewage and fishery in these regions (Zeng et al., 2009) as sewage and fertilizer usually have enriched $\delta^{15}\text{N}$ -TDN signature and high COD (Vizzini et al., 2005).

Further evidence of the role of Q_{net} comes from 1) the significant positive relationships between monthly mean Q_{net} and $a(350)$, DOC, COD, Chl- a , F_{max} of C1-C3 and C7, and %C2-%C3. This indicated that terrestrial and anthropogenic CDOM increased with Q_{net} as C3 is a typical terrestrial humic-rich component and the spectral shape of C2 is highly close to that of household sewage (Zhou et al., 2016). 2) The negative

relationships between mean Q_{net} and $a(250)/a(365)$, $S_{275-295}$, and %C4-%C5 (Fig. 6; Fig. 8). This suggested that prolonged water residence time resulted from lower Q_{net} in the southeastern sub-watersheds possibly resulted in elevated accumulation of autochthonous protein-like components in these watersheds relative to the other sub-watersheds. 3) the positive relationships between the products of $Q_{\text{net}} \times$ urban land cover, $Q_{\text{net}} \times$ GDP, and $Q_{\text{net}} \times$ population density and mean $a(350)$, DOC, COD, Chl- a , C1-C3, and %C2-%C3, and 4) the negative relationships between the products of $Q_{\text{net}} \times$ urban land cover, $Q_{\text{net}} \times$ GDP, and $Q_{\text{net}} \times$ population density and $a(250)/a(365)$, $S_{275-295}$, and %C4 (Fig. 7; Table S4). This suggests that the products of Q_{net} and anthropogenic indices controls largely on DOC concentrations and the optical properties of CDOM. Q_{net} serves as a surrogate of the net inflow discharge from the individual sub-watersheds while the products of $Q_{\text{net}} \times$ urban land cover, $Q_{\text{net}} \times$ GDP, and $Q_{\text{net}} \times$ population density is a tracer of the extent of household sewage discharge from the residential areas of individual sub-watersheds. The higher $Q_{\text{net}} \times$ urban land cover, $Q_{\text{net}} \times$ GDP, and $Q_{\text{net}} \times$ population density in the northwestern sub-watersheds relative to the remaining sub-watersheds can therefore explain the strong terrestrial and anthropogenic CDOM input here. In comparison, the higher urban land cover, GDP, and population density in the southeastern sub-watersheds (e.g. Yangchengdingmao and Hangjiahu; Fig. 1; Fig. S3; Table S2) may presumably resulted in higher load of household sewage containing high concentration of CDOM. However, the negative Q_{net} in these regions implies that backflow runoff discharged from the lake to the connecting channels was higher than inflow runoff from the channels to the lake. This resulted in negative $Q_{\text{net}} \times$ urban land cover, $Q_{\text{net}} \times$ GDP, and $Q_{\text{net}} \times$ population density, and

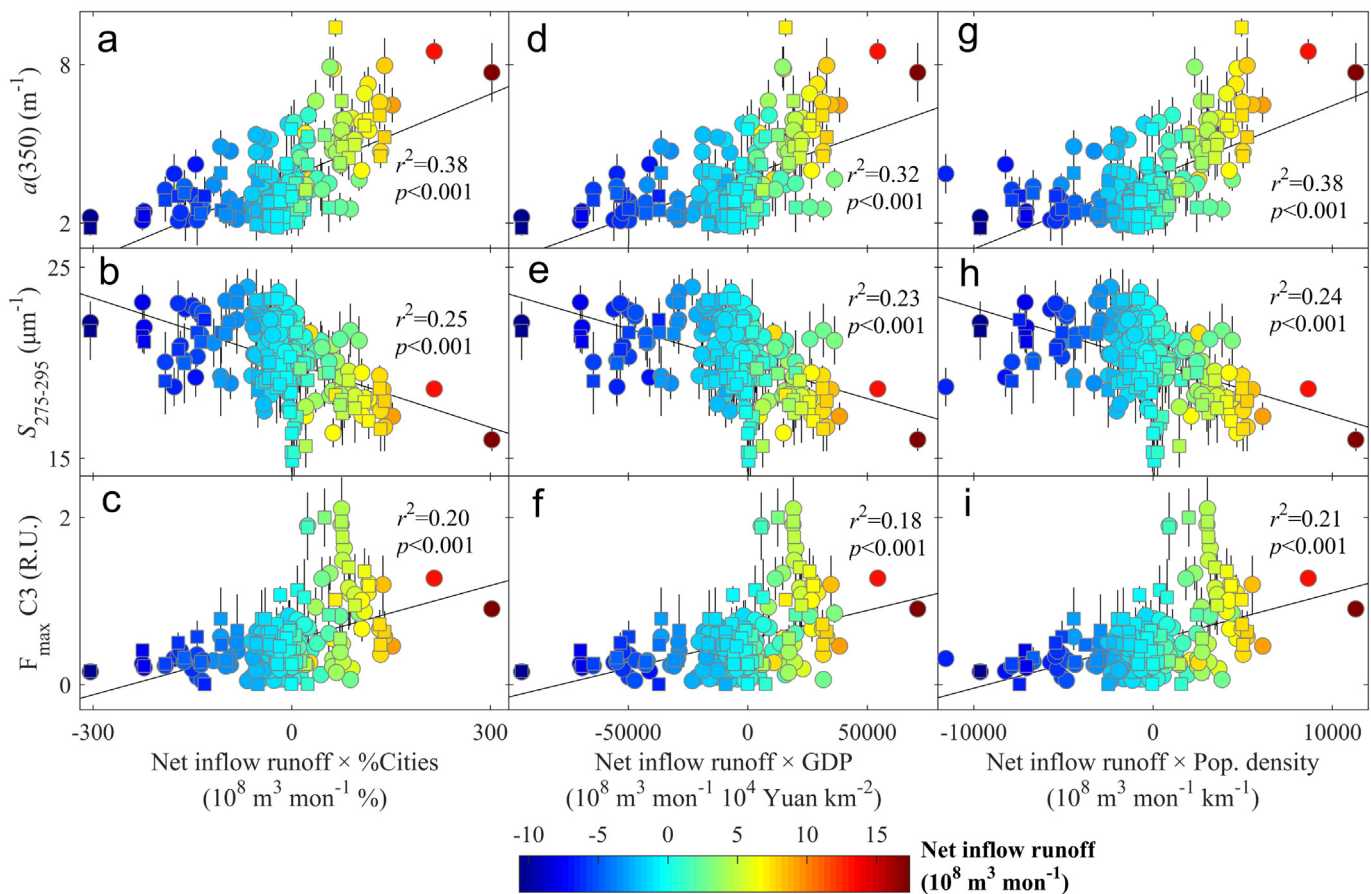


Fig. 7. Relationships between the products of monthly net inflow runoff ($Q_{\text{net}} \times$ urban percentage (%Cities) of land cover and CDOM absorption coefficient $a(350)$ (a), absorption spectral slope $S_{275-295}$ (b), F_{max} of PARAFAC-derived terrestrial humic-like C3 (c), between the products of monthly $Q_{\text{net}} \times$ gross domestic products (GDP) and $a(350)$ (d), $S_{275-295}$ (e), F_{max} of C3 (f), and between the products of $Q_{\text{net}} \times$ population density and $a(350)$ (g), $S_{275-295}$ (h), F_{max} of C3 (i) for the samples collected from five lake regions and the connecting channels delineated by white dashed lines as shown in Fig. 1. Circles: samples collected from the lake; quadrates: samples collected from the channels. Error bars in all panels represent ± 1 S.D. of samples collected from the five lake regions.

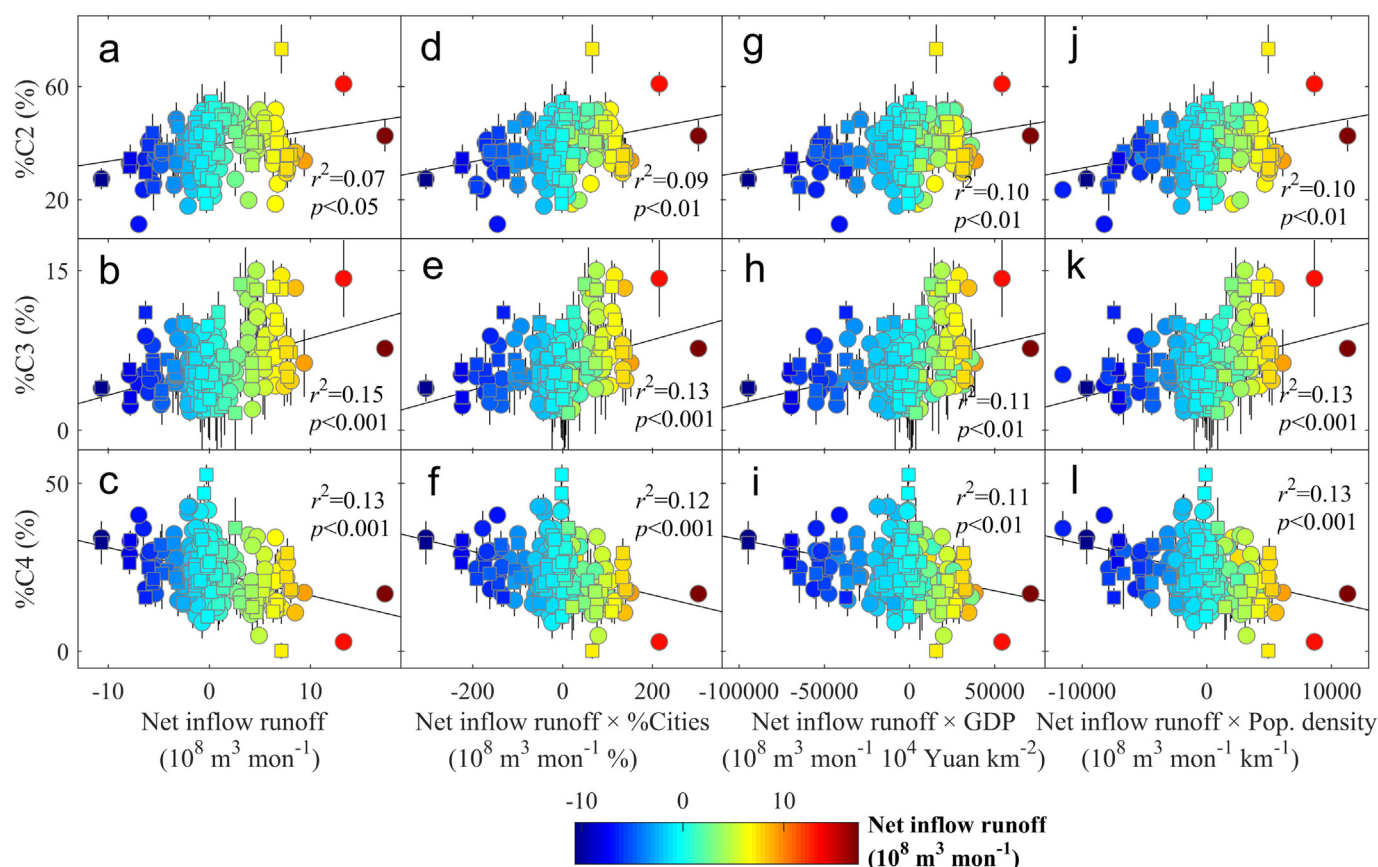


Fig. 8. Relationships between monthly net inflow runoff (Q_{net}) and the contribution percentages of PARAFAC components C2–C4 (%C2–%C4; a–c), and between the products of monthly net inflow runoff (Q_{net}) \times urban land cover (%Cities) and %C2–%C4 (d–f), and between the products of monthly Q_{net} \times gross domestic products (GDP) and %C2–%C4 (g–i), and between the products of monthly Q_{net} \times population density and %C2–%C4 (j–l) for the samples collected from five lake regions and the connecting channels delineated by white dashed lines as shown in Fig. 1. Circles: samples collected from the lake; quadrates: samples collected from the channels. Error bars in all panels represent ± 1 S.D. of samples collected from the five lake regions.

thereby explains the relatively low $a(350)$, DOC, COD, Chl- a , and F_{max} of C1–C7 in the southeastern lake regions (Fig. 4; Fig. S6). Samples collected from the channels in different sub-watersheds all share strong anthropogenic EEMs signals despite their distinct optical properties (Fig. S4; Table S3). Our results therefore suggested that in the Lake Taihu watersheds, Q_{net} serves as an indicator of anthropogenic disturbance influencing the optical characterizations of CDOM (Williams et al., 2016; Williams et al., 2010) in the lake and the connecting channels.

Our results indicated that riverine DOM primarily contributed to the DOM pool in Lake Taihu. This is supported by 1) the mean value of $\sim 26.2\%$ of $\delta^{13}\text{C-DOM}$ of the whole lake and 2) the declining $a(350)$, DOC, COD, Chl- a , $\delta^{15}\text{N-TDN}$, F_{max} of humic-like components C1, C3, and C7, and C_{humics} from northwestern to the southeastern lake regions (Fig. 5; Fig. S6). 3) Although terrestrial humic-like signal C3 represents limited contribution percentage to the summed F_{max} of the seven PARAFAC components, it explained $>56\%$ of the variability in DOC concentrations (Fig. S7). In comparison, protein-like components, some of which is produced by phytoplankton degradation (Fig. 4) (Stedmon et al., 2007; Williams et al., 2010; Yamashita et al., 2008; Yao et al., 2011) contributed only marginally to the total DOM pool in the lake (Fig. S7). 4) The major contribution percentages of lignin peaks with molecular formulas assigned for the headwater sample, the inflowing river and lake samples in the Huxi watershed, and the central lake sample (Fig. 9; Table S5). All the samples were enriched in nitrogen and the limited contribution percentage of proteins and lipids for the central lake sample provide direct evidence that riverine DOM contributed primarily to the DOM pool in Lake Taihu (Fig. 9; Table S5). The significant positive relationship between Chl- a and the red-shifted microbial humic-like C7 (Fig. S11) suggested that algal degradation is a potential

important source to CDOM pool in the lake. This agrees with recent studies that the degradation of algae cells in the summer impacted importantly to the CDOM optical properties in the lake (Zhang et al., 2009; Zhou et al., 2015a). A recent study have further suggested that CDOM released from lakebed prewewater potentially contributed importantly to the CDOM pool in the overlying water column of the large and shallow lake (Xu et al., 2016).

In the large and shallow Lake Taihu, the prolonged water retention time and high UV–vis underwater light availability in the eastern bays compared to other regions (Shi et al., 2014) likely enhance the photodegradation of terrestrial-derived humic-rich CDOM in these regions (Zhang et al., 2013). We did not consider water flow direction in the lake as it varies over time (and is difficult to estimate being affected by prevailing wind direction, anthropogenic, and tidal conditions (Qin et al., 2007)). However, the strong relationships between monthly mean Q_{net} and $a(350)$, DOC, COD, Chl- a , $S_{275-295}$, F_{max} of C1–C3 and C7, and %C2–%C4 (Fig. 6; Fig. 8; Table 1; Table S4) suggest that Q_{net} from channels connecting to the lake was the primary factor influencing the CDOM optical characteristics. Although urban land cover, GDP, and population density in the five sub-watershed changes remarkably over the past decade, their relative spatial distribution patterns are relative stable over time with the highest urban land cover, GDP, and population density found in the Wuchengxiyu and the lowest in the Zhexi sub-watershed (Fig. S3; Table S2). This strongly supported that Q_{net} rather than urban land cover, GDP, or population density controls the optical property of CDOM in the fluvial plain Lake Taihu watershed. This is further substantiated by the multiple regression results that adding urban land cover, GDP, and population density to Q_{net} as independent variables does not increase but rather decrease the determination

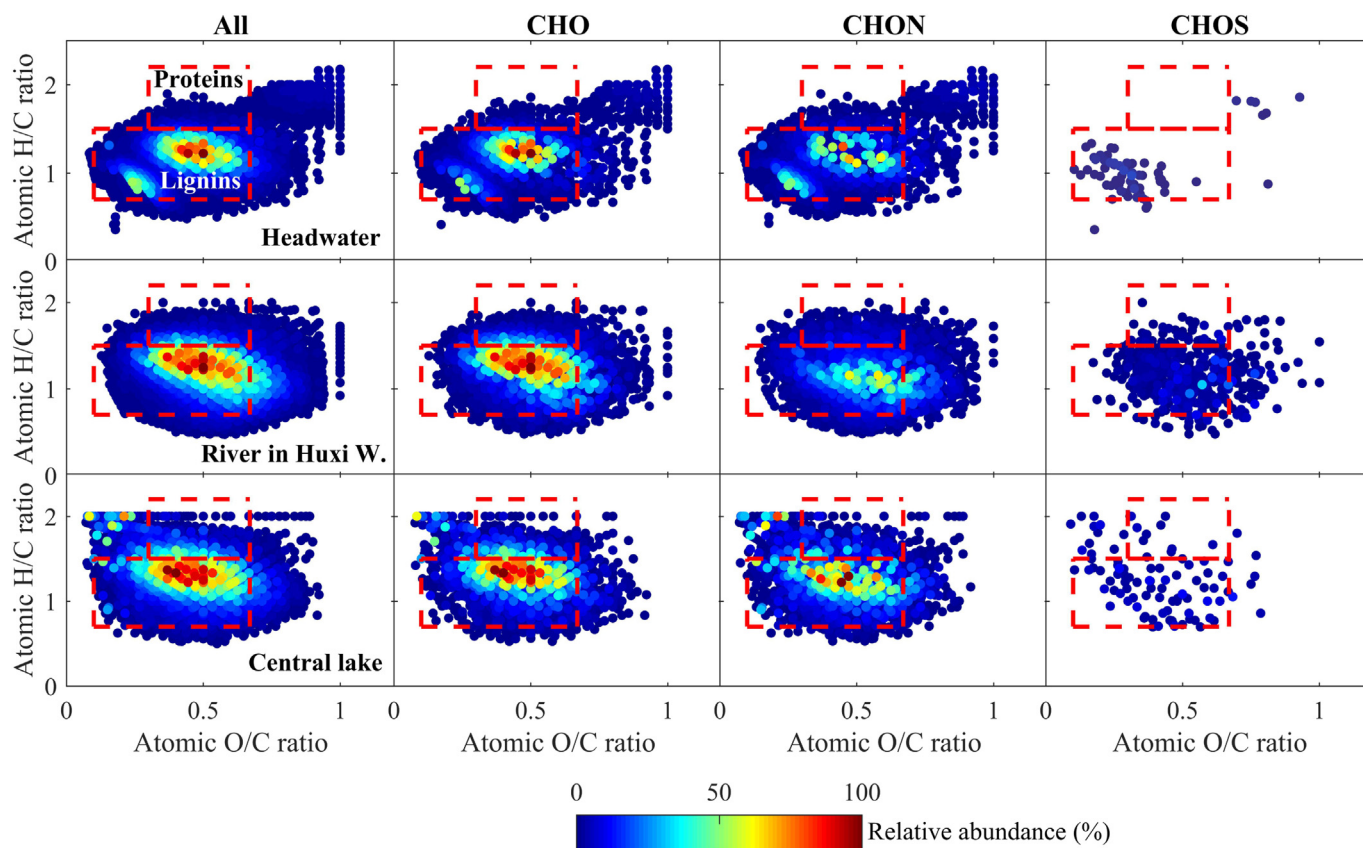


Fig. 9. van Krevelen diagrams of assigned molecular formulas of headwater DOM (upper row), river samples in the Huxi watershed (see Fig. 1 for the location of the Huxi watershed, middle row), and central Lake Taihu DOM (lower row) sample. Also shown are the van Krevelen diagrams of the distributions of all (1st column), carbohydrates (CHO, 2nd column), nitrogen-containing compounds (CHON, 3rd column), and sulphur-containing compounds (CHOS, 4th column) formulas.

coefficients compared with simple linear fittings between Q_{net} and CDOM-related variables (Table 1; Fig. 6; Fig. 7).

CDOM fluorescence may serve as a reasonable good surrogate for biological oxygen demand (BOD), COD, and total nitrogen (Hur and Cho, 2012). The important role of Q_{net} for the amount and composition of CDOM demonstrated here call for a close monitoring of the inflow and backflow in the major channels to and from the lake in order to develop advanced water quality management schemes for the lake and for decisions on how to control the input. At present, the resolution for inflow and backflow time series for the whole lake and watershed are only available on monthly and sub-watershed bases. During the algal bloom seasons, high frequency monitoring of Q_{net} from individual channels, especially those with high terrestrial CDOM concentrations, would be useful as early warming indicator of high CDOM in the lake reducing the usability of the water as a drinking water resource (Qin et al., 2015). Moreover, as freshly organic and inorganic matter inputs to lake ecosystems are exposed to photochemical and biological degradation (Hur et al., 2011; Stedmon and Markager, 2005b). The degradation processes can fuel the outgassing of greenhouse gases (Weyhenmeyer et al., 2015), future work should focus on how terrestrial CDOM input coming with the connecting channels impacts greenhouse gas emissions from fluvial plain lake ecosystems.

Acknowledgments

This study was jointly funded by the National Natural Science Foundation of China (grants 41325001, 41621002, and 41771514), the Key Research Program of Frontier Sciences, Chinese Academy of Sciences (QYZDB-SSW-DQC016), and NIGLAS Foundation (NIGLAS2017QD08). Erik Jeppesen was supported by the MARS project (Managing Aquatic ecosystems and water Resources under multiple Stress) funded under

the 7th EU Framework Programme, Theme 6 (Environment including Climate Change), Contract No.: 603378 (<http://www.mars-project.eu>) and AU Water Technology Centre (WATEC). We would like to express our deep thanks to Anne Mette Poulsen from Aarhus University (grants 603378) for editorial assistance. We would also like to thank Zhiqiang Shi, Yan Yin, Mingzhu Wang, Xiaohan Liu, Longqing Feng, Jingchen Xue, Zhong Xia, Hao Jiang, and Chengying Zhang for their help with field sample collection and laboratory measurements. The authors are grateful to Dr. Kevin Thomas and the two anonymous reviewers for their constructive comments and suggestions.

Appendix A. Supplementary data

Supplementary data to this article can be found online at <https://doi.org/10.1016/j.scitotenv.2018.05.180>.

References

- Andersson, C.A., Bro, R., 2000. The N-way toolbox for MATLAB. *Chemom. Intell. Lab. Syst.* 52, 1–4.
- Corilo, Y., 2015. *EnviroOrg*. Florida State University.
- Davidson, T.A., Audet, J., Jeppesen, E., Landkildehus, F., Lauridsen, T.L., Søndergaard, M., et al., 2018. Synergy between nutrients and warming enhances methane ebullition from experimental lakes. *Nat. Clim. Chang.* 8, 156–160.
- Duan, H.T., Ma, R.H., Loisselle, S.A., Shen, Q.S., Yin, H.B., Zhang, Y.C., 2014. Optical characterization of black water blooms in eutrophic waters. *Sci. Total Environ.* 482–483, 174–183.
- Fichot, C.G., Benner, R., 2012. The spectral slope coefficient of chromophoric dissolved organic matter (S275–295) as a tracer of terrigenous dissolved organic carbon in river-influenced ocean margins. *Limnol. Oceanogr.* 57, 1453–1466.
- Graeber, D., Gelbrecht, J., Pusch, M.T., Anlanger, C., von Schiller, D., 2012. Agriculture has changed the amount and composition of dissolved organic matter in central European headwater streams. *Sci. Total Environ.* 438, 435–446.
- Guo, W., Yang, L., Zhai, W., Chen, W., Osburn, C.L., Huang, X., et al., 2014. Runoff-mediated seasonal oscillation in the dynamics of dissolved organic matter in different branches

- of a large bifurcated estuary—the Changjiang Estuary. *J. Geophys. Res. Biogeosci.* 119, 776–793.
- Helms, J.R., Stubbins, A., Ritchie, J.D., Minor, E.C., Kieber, D.J., Mopper, K., 2008. Absorption spectral slopes and slope ratios as indicators of molecular weight, source, and photobleaching of chromophoric dissolved organic matter. *Limnol. Oceanogr.* 53, 955–969.
- Hood, E., Fellman, J., Spencer, R.G., Hernes, P.J., Edwards, R., D'Amore, D., et al., 2009. Glaciers as a source of ancient and labile organic matter to the marine environment. *Nature* 462, 1044–1047.
- Huang, C., Yao, L., Zhang, Y., Huang, T., Zhang, M., Zhu, A.X., et al., 2017. Spatial and temporal variation in autochthonous and allochthonous contributors to increased organic carbon and nitrogen burial in a plateau lake. *Sci. Total Environ.* 603–604, 390–400.
- Hur, J., Cho, J., 2012. Prediction of BOD, COD, and total nitrogen concentrations in a typical urban river using a fluorescence excitation–emission matrix with PARAFAC and UV absorption indices. *Sensors (Basel)* 12, 972–986.
- Hur, J., Jung, K.Y., Jung, Y.M., 2011. Characterization of spectral responses of humic substances upon UV irradiation using two-dimensional correlation spectroscopy. *Water Res.* 45, 2965–2974.
- Kellerman, A.M., Kothawala, D.N., Dittmar, T., Tranvik, L.J., 2015. Persistence of dissolved organic matter in lakes related to its molecular characteristics. *Nat. Geosci.* 8, 454–457.
- Kothawala, D.N., Murphy, K.R., Stedmon, C.A., Weyhenmeyer, G.A., Tranvik, L.J., 2013. Inner filter correction of dissolved organic matter fluorescence. *Limnol. Oceanogr. Methods* 11, 616–630.
- Kothawala, D.N., Stedmon, C.A., Muller, R.A., Weyhenmeyer, G.A., Kohler, S.J., Tranvik, L.J., 2014. Controls of dissolved organic matter quality: evidence from a large-scale boreal lake survey. *Glob. Chang. Biol.* 20, 1101–1114.
- Kowalczyk, P., Tilstone, G.H., Zablocka, M., Röttgers, R., Thomas, R., 2013. Composition of dissolved organic matter along an Atlantic meridional transect from fluorescence spectroscopy and parallel factor analysis. *Mar. Chem.* 157, 170–184.
- Lawaetz, A.J., Stedmon, C.A., 2009. Fluorescence intensity calibration using the Raman scatter peak of water. *Appl. Spectrosc.* 63, 936–940.
- Le, C., Lehrter, J.C., Hu, C., Schaeffer, B., Macintyre, H., Hagy, J.D., et al., 2015. Relation between inherent optical properties and land use and land cover across Gulf Coast estuaries. *Limnol. Oceanogr.* 60, 920–933.
- Li, P., Lee, S.H., Lee, S.H., Lee, J.B., Lee, Y.K., Shin, H.S., et al., 2016. Seasonal and storm-driven changes in chemical composition of dissolved organic matter: a case study of a reservoir and its forested tributaries. *Environ. Sci. Pollut. Res.* 23, 24834–24845.
- Liu, J., Liu, M., Tian, H., Zhuang, D., Zhang, Z., Zhang, W., et al., 2005. Spatial and temporal patterns of China's cropland during 1990–2000: an analysis based on Landsat TM data. *Remote Sens. Environ.* 98, 442–456.
- Mcknight, D.M., Boyer, E.W., Westerhoff, P.K., Doran, P.T., Kulbe, T., Andersen, D.T., 2001. Spectrofluorometric characterization of dissolved organic matter for indication of precursor organic material and aromaticity. *Limnol. Oceanogr.* 46, 38–48.
- Murphy, K.R., Stedmon, C.A., Waite, T.D., Ruiz, G.M., 2008. Distinguishing between terrestrial and autochthonous organic matter sources in marine environments using fluorescence spectroscopy. *Mar. Chem.* 108, 40–58.
- Murphy, K.R., Hambly, A., Singh, S., Henderson, R.K., Baker, A., Stuetz, R., et al., 2011. Organic matter fluorescence in municipal water recycling schemes: toward a unified PARAFAC model. *Environ. Sci. Technol.* 45, 2909–2916.
- Murphy, K.R., Stedmon, C.A., Graeber, D., Bro, R., 2013. Fluorescence spectroscopy and multi-way techniques. *PARAFAC. Anal. Methods* 5, 6557–6566.
- Murphy, K.R., Stedmon, C.A., Wenig, P., Bro, R., 2014. OpenFluor—an online spectral library of auto-fluorescence by organic compounds in the environment. *Anal. Methods* 6, 658–661.
- Ohno, T., Parr, T.B., Gruselle, M.C., Fernandez, I.J., Sleighter, R.L., Hatcher, P.G., 2014. Molecular composition and biodegradability of soil organic matter: a case study comparing two new England forest types. *Environ. Sci. Technol.* 48, 7229–7236.
- Osburn, C.L., Handsel, L.T., Peierls, B.L., Paerl, H., 2016. Predicting sources of dissolved organic nitrogen to an estuary from an agro-urban coastal watershed. *Environ. Sci. Technol.* 50, 8473–8484.
- Paerl, H.W., Hall, N.S., Peierls, B.L., Rossignol, K.L., Joyner, A.R., 2013. Hydrologic variability and its control of phytoplankton community structure and function in two shallow, coastal, lagoonal ecosystems: the Neuse and New River estuaries, North Carolina, USA. *Estuar. Coasts* 37, 31–45.
- Qin, B., Xu, P., Wu, Q., Luo, L., Zhang, Y., 2007. Environmental issues of Lake Taihu, China. *Hydrobiologia* 581, 3–14.
- Qin, B., Li, W., Zhu, G., Zhang, Y., Wu, T., Gao, G., 2015. Cyanobacterial bloom management through integrated monitoring and forecasting in large shallow eutrophic Lake Taihu (China). *J. Hazard. Mater.* 287, 356–363.
- Shi, K., Zhang, Y., Liu, X., Wang, M., Qin, B., 2014. Remote sensing of diffuse attenuation coefficient of photosynthetically active radiation in Lake Taihu using MERIS data. *Remote Sens. Environ.* 140, 365–377.
- Shutova, Y., Baker, A., Bridgeman, J., Henderson, R.K., 2014. Spectroscopic characterisation of dissolved organic matter changes in drinking water treatment: from PARAFAC analysis to online monitoring wavelengths. *Water Res.* 54, 159–169.
- Spencer, R.G.M., Guo, W., Raymond, P.A., Dittmar, T., Hood, E., Fellman, J., et al., 2014. Source and biolability of ancient dissolved organic matter in glacier and lake ecosystems on the Tibetan plateau. *Geochim. Cosmochim. Acta* 142, 64–74.
- Stedmon, C.A., Bro, R., 2008. Characterizing dissolved organic matter fluorescence with parallel factor analysis: a tutorial. *Limnol. Oceanogr. Methods* 6, 572–579.
- Stedmon, C.A., Markager, S., 2005a. Resolving the variability in dissolved organic matter fluorescence in a temperate estuary and its catchment using PARAFAC analysis. *Limnol. Oceanogr.* 50, 686–697.
- Stedmon, C.A., Markager, S., 2005b. Tracing the production and degradation of autochthonous fractions of dissolved organic matter by fluorescence analysis. *Limnol. Oceanogr.* 50, 1415–1426.
- Stedmon, C.A., Thomas, D.N., Granskog, M., Kaartokallio, H., Papadimitriou, S., Kuosa, H., 2007. Characteristics of dissolved organic matter in Baltic coastal sea ice: allochthonous or autochthonous origins? *Environ. Sci. Technol.* 41, 7273–7279.
- Stubbins, A., Spencer, R.G.M., Chen, H., Hatcher, P.G., Mopper, K., Hernes, P.J., et al., 2010. Illuminated darkness: molecular signatures of Congo River dissolved organic matter and its photochemical alteration as revealed by ultrahigh precision mass spectrometry. *Limnol. Oceanogr.* 55, 1467–1477.
- Tang, X., Gao, G., Chao, J., Wang, X., Zhu, G., Qin, B., 2010. Dynamics of organic-aggregate-bacterial communities and related environmental factors in Lake Taihu, a large eutrophic shallow lake in China. *Limnol. Oceanogr.* 55, 469–480.
- Tomlinson, A., Driks, M., Brookes, J.D., 2016. The role of phytoplankton as pre-cursors for disinfection by-product formation upon chlorination. *Water Res.* 102, 229–240.
- Vizzini, S., Savona, B., Chi, T.D., Mazzola, A., 2005. Spatial variability of stable carbon and nitrogen isotope ratios in a Mediterranean coastal lagoon. *Hydrobiologia* 550, 73–82.
- Weyhenmeyer, G.A., Kosten, S., Wallin, M.B., Tranvik, L.J., Jeppesen, E., Roland, F., 2015. Significant fraction of CO₂ emissions from boreal lakes derived from hydrologic inorganic carbon inputs. *Nat. Geosci.* 8, 933–936.
- Williams, C.J., Yamashita, Y., Wilson, H.F., Jaffé, R., Xenopoulos, M.A., 2010. Unraveling the role of land use and microbial activity in shaping dissolved organic matter characteristics in stream ecosystems. *Limnol. Oceanogr.* 55, 1159–1171.
- Williams, C.J., Frost, P.C., Morales-Williams, A.M., Larson, J.H., Richardson, W.B., Chiandret, A.S., et al., 2016. Human activities cause distinct dissolved organic matter composition across freshwater ecosystems. *Glob. Chang. Biol.* 22, 613–626.
- Xu, H., Guo, L., Jiang, H., 2016. Depth-dependent variations of sedimentary dissolved organic matter composition in a eutrophic lake: implications for lake restoration. *Chemosphere* 145, 551–559.
- Yamashita, Y., Jaffé, R., Maie, N., Tanoue, E., 2008. Assessing the dynamics of dissolved organic matter (DOM) in coastal environments by excitation emission matrix fluorescence and parallel factor analysis (EEM-PARAFAC). *Limnol. Oceanogr.* 53, 1900–1908.
- Yamashita, Y., Maie, N., Briceno, H., Jaffé, R., 2010. Optical characterization of dissolved organic matter in tropical rivers of the Guayana Shield, Venezuela. *J. Geophys. Res. Biogeosci.* 115, G00F10.
- Yamashita, Y., Boyer, J.N., Jaffé, R., 2013. Evaluating the distribution of terrestrial dissolved organic matter in a complex coastal ecosystem using fluorescence spectroscopy. *Cont. Shelf Res.* 66, 136–144.
- Yang, L., Guo, W., Chen, N., Hong, H., Huang, J., Xu, J., et al., 2013. Influence of a summer storm event on the flux and composition of dissolved organic matter in a subtropical river, China. *Appl. Geochem.* 28, 164–171.
- Yao, X., Zhang, Y., Zhu, G., Qin, B., Feng, L., Cai, L., et al., 2011. Resolving the variability of CDOM fluorescence to differentiate the sources and fate of DOM in Lake Taihu and its tributaries. *Chemosphere* 82, 145–155.
- Zeng, Q.F., Kong, F.X., Zhang, E.L., Tan, X., Wu, X.D., 2009. Seasonality of stable carbon and nitrogen isotopes within the pelagic food web of Taihu Lake. *Ann. Limnol. Int. J. Limnol.* 44, 1–6.
- Zhang, Y., van Dijk, M.A., Liu, M., Zhu, G., Qin, B., 2009. The contribution of phytoplankton degradation to chromophoric dissolved organic matter (CDOM) in eutrophic shallow lakes: field and experimental evidence. *Water Res.* 43, 4685–4697.
- Zhang, Y., Yin, Y., Liu, X., Shi, Z., Feng, L., Liu, M., et al., 2011. Spatial-seasonal dynamics of chromophoric dissolved organic matter in Lake Taihu, a large eutrophic, shallow lake in China. *Org. Geochem.* 42, 510–519.
- Zhang, Y.L., Liu, X.H., Osburn, C.L., Wang, M.Z., Qin, B.Q., Zhou, Y.Q., 2013. Photobleaching response of different sources of chromophoric dissolved organic matter exposed to natural solar radiation using absorption and excitation-emission matrix spectra. *PLoS One* 8, e77515.
- Zhao, Y., Song, K., Li, S., Ma, J., Wen, Z., 2016. Characterization of CDOM from urban waters in northern-northeastern China using excitation-emission matrix fluorescence and parallel factor analysis. *Environ. Sci. Pollut. Res.* 23, 15381–15394.
- Zhao, Y., Song, K., Shang, Y., Shao, T., Wen, Z., Lv, L., 2017. Characterization of CDOM of river waters in China using fluorescence excitation-emission matrix and regional integration techniques. *J. Geophys. Res. Biogeosci.* 122, 1940–1953.
- Zhou, Y., Jeppesen, E., Zhang, Y., Niu, C., Shi, K., Liu, X., et al., 2015a. Chromophoric dissolved organic matter of black waters in a highly eutrophic Chinese lake: freshly produced from algal scums? *J. Hazard. Mater.* 299, 222–230.
- Zhou, Y., Zhang, Y., Shi, K., Liu, X., Niu, C., 2015b. Dynamics of chromophoric dissolved organic matter influenced by hydrological conditions in a large, shallow, and eutrophic lake in China. *Environ. Sci. Pollut. Res.* 22, 12992–13003.
- Zhou, Y., Jeppesen, E., Zhang, Y., Shi, K., Liu, X., Zhu, G., 2016. Dissolved organic matter fluorescence at wavelength 275/342 nm as a key indicator for detection of point-source contamination in a large Chinese drinking water lake. *Chemosphere* 144, 503–509.
- Zhu, M., Paerl, H.W., Zhu, G., Wu, T., Li, W., Shi, K., et al., 2014. The role of tropical cyclones in stimulating cyanobacterial (*Microcystis* spp.) blooms in hypertrophic Lake Taihu, China. *Harmful Algae* 39, 310–321.